J Math Chem (2012) 50:2527–2557
DOI 10.1007/s10910-012-0047-1

ORIGINAL PAPER

A meta-analysis of studies using MR spectroscopy for evaluating suspicious lesions after radiation therapy of primary brain tumors

Dževad Belkić · Karen Belkić

Received: 30 May 2012 / Accepted: 5 July 2012 / Published online: 14 August 2012

Abstract Primary brain tumors frequently return after radiation therapy (RT). In addition, RT can provoke changes in brain tissue that are difficult to distinguish from tumor recurrence using magnetic resonance imaging. Magnetic resonance spectroscopy (MRS) and spectroscopic imaging (MRSI) have been applied quite extensively with the aim of better differentiating recurrent brain tumors from radiation necrosis. To the best of our knowledge, however, there have not been any published papers within this context in which the results of MRS and MRSI have been analyzed in a comprehensive, integrative manner. Through meta-analysis, the present paper aims to determine which metabolite concentration ratios could potentially be the most reliable for differentiating post-RT recurrent brain tumor from radiation necrosis. We systematically reviewed the literature to find empirical studies of patients treated with RT for primary malignant brain tumors, and who developed a new lesion post-RT, which was assessed using MRS or MRSI. Reported data from individual patients were entered into a single data set for detailed statistical analysis. Six articles were identified that fulfilled the criteria for inclusion in the present study. From these, quantitative MRS/MRSI data were provided for sixty-three patients with recurrent brain tumors and for thirty-eight patients with radiation necrosis. Higher choline to creatine and choline to N-Acetyl Aspartate (NAA) concentration ratios were associated with a significantly greater

Dž. Belkić (✉) · K. Belkić
Department of Oncology and Pathology, Karolinska Institute, P.O. Box 260,
171776 Stockholm, Sweden
e-mail: Dzevad.Belkic@ki.se

K. Belkić
School of Community and Global Health, Claremont Graduate University, Claremont, CA, USA

K. Belkić
Institute for Health Promotion and Disease Prevention Research, University of Southern California
School of Medicine, Los Angeles, CA, USA

likelihood of recurrent tumor, as opposed to radiation necrosis. This was found with and without statistical adjustment for high grade of the primary tumor, echo time (TE) and static magnetic field strength (B_0). Higher NAA to creatine and lactate to choline concentration ratios were associated with a significantly greater likelihood of radiation necrosis as opposed to recurrent tumor, both with and without adjustment for tumor grade, TE and B_0. Only the lactate to choline concentration ratio yielded 100 % correct prediction of all the cases for which data were available. However, data on lactate to choline concentration ratios were available for less than one-third of the patients; these were all recorded at long TE, at which most of the major signal components for the other metabolites have decayed to the level of background noise. No cutpoint values for the choline to creatine or choline to NAA concentration ratios could be identified that optimally distinguished recurrent tumor from radiation necrosis. We conclude that metabolite concentration ratios assessed within MRS/MRSI could potentially be helpful in distinguishing tumor recurrence from radiation necrosis. However, optimal distinction of these two entities has not yet been provided, mainly because of the nearly exclusive reliance upon the conventional estimations by post-processing of Fourier spectral envelopes with various fitting computations that are all equivocal. In order to more accurately identify recurrent brain tumor post-RT as opposed to radiation-induced changes, a more advanced and unequivocal mathematical approach for quantification of MRS/MRSI signals is needed. The answer of choice to this quest is offered by the universally applicable method of rational functions from the mathematical theory of approximations. The most salient feature of rational functions is their capability to accurately describe the essential behavior of generic systems by means of the least number of quantifying parameters, as an indispensable prerequisite for a parsimonious mathematical modeling. The most established rational response function, which has passed the test of time across interdisciplinary research, is the Padé approximant. Adapted to signal processing and accordingly called the fast Padé transform, this versatile method is the optimal spectral analyzer for MRS/MRSI data. It is within such a strategy that the questions addressed in this study could be answered in an adequate manner.

Keywords Radiation therapy · Gliomas · Radiation necrosis · Magnetic resonance spectroscopy · Signal processing

Abbreviations

B_0	Magnetic field strength
CE	Contrast enhancing
Chemotx	Chemotherapy
Cho	Choline
CNS	Central nervous system
Cr	Creatine
CRT	Conformal radiation therapy
EBRT	External beam radiotherapy
FFT	Fast Fourier transform
FID	Free induction decay
FPT	Fast Padé transform

Gy	Gray
Lac	Lactate
M	Months
MRI	Magnetic resonance imaging
MRS	Magnetic resonance spectroscopy
MRSI	Magnetic resonance spectroscopic imaging
ms	Milliseconds
NAA	N-acetyl aspartate
NPV	Negative predictive value
ppm	Parts per million
PPV	Positive predictive value
RN	Radiation necrosis
RT	Radiation therapy
RTu	Recurrent tumor
SRS	Stereotactic radiosurgery
T	Tesla
TE	Echo time
Tx	Therapy or treated
U	University
VOI	Voxel of interest
vs	Versus

1 Introduction

Primary brain tumors frequently return after radiation therapy (RT) [1]. In addition, RT can provoke changes in brain tissue that are difficult to distinguish from tumor recurrence [2,3]. Both radiation necrosis and tumor recurrence typically present as new contrast enhancing (CE) lesions and/or as a new region of T_2-weighted hyper-intensity on magnetic resonance imaging (MRI) [2,3].

The sensitivity of MRI is excellent, with most pathology being detected, but its specificity is insufficient for distinguishing cancer from benign tumors or other non-malignant lesions [4]. By detecting the metabolic features of cancer, magnetic resonance spectroscopy (MRS) and magnetic resonance spectroscopic imaging (MRSI) can improve the specificity of MRI. Both MRS and MRSI have been applied quite extensively with the aim of better differentiating recurrent brain tumors from radiation-induced non-malignant changes, most commonly, radiation necrosis[1] [1–20].

Choline concentration levels, reflecting phospholipid metabolism of cell membranes, and as markers for membrane damage, cellular proliferation and cell density, are generally found to rise prior to the appearance of contrast enhancement due to recurrent glioma. Choline (Cho) has its resonant frequency at ∼3.2 ppm (parts per million). Nitrogen acetyl aspartate (NAA), which resonates at ∼2.0 ppm is a marker of number and viability of neurons. Ratios of Cho to NAA have been reported to be

[1] Necrosis denotes death of cellular material or a section of tissue with extensive damage and inflammation. This is most often due to some external perturbation, e.g. exposure to ionizing radiation.

higher in recurrent brain tumors than in radiation injury[2] [2,15,16,18]. Creatine (Cr) which resonates at ∼3.0 ppm is a marker of cerebral energy metabolism. Elevated ratios of Cho to Cr have also been reported to help distinguish recurrent brain tumors from radiation injury [7–9,15,19,20]. Due to the predominance of anaerobic glycolysis, a lactate doublet at around 1.3 ppm is often seen in brain tumors [21]. On the other hand, high levels of lactate (Lac) are reported in association with necrotic processes [22], including radiation necrosis. Significantly higher Lac to Cr ratios in radiation necrosis have been found compared to brain tumors [7], but higher Lac to Cho ratios were reported in recurrent brain tumors [9]. In a small series of patients treated by RT for gliomas, elevated Lac to Cr ratios were found in association with tumor recurrence [17].

To the best of our knowledge, there have not been any published papers in which the above-cited results have been analyzed in a comprehensive, integrative manner. Motivated by its urgent clinical importance, the present paper aims to fill this gap by performing a meta-analysis based upon a logistic probability predictor using the available published data on this topic. We seek to determine which metabolite ratios could be the most reliable for differentiating post-RT recurrent brain tumor from radiation necrosis. Since clinicians seek to make decisions based upon metabolite ratio cutpoints values, we will assess the usefulness of this practice in comparison to the results employing the raw input data. Alternatively, our analysis will aim to point at the next needed steps in MRS/MRSI studies on this topic, in order to optimize the accuracy with which post-RT recurrent brain tumor is distinguished from radiation-induced changes. Such distinctions are not possible on the level of the raw, measured data. To this end, mathematical methods using spectral analysis of proven reliability and validity are needed. The optimal signal processor for quantifying MRS/MRSI data is the fast Padé transform (FPT) [6], which can correctly assess the role of metabolite concentration ratios in general and also in the context of the mentioned post-RT distinction between tumor recurrence and radiation necrosis.

2 Methods

2.1 Search strategy

We performed a systematic, comprehensive search of the medical literature to find all relevant published articles, using two of the most reliable search engines in medicine: OVID MEDLINE and PUBMED. The following three search terms as clauses were simultaneously included:

- magnetic resonance spectroscopy,
- radiation therapy,
- brain tumor.

[2] In the MRS literature, a notion such as “choline to creatine ratio” or Cho/Cr actually refers to [Cho]/[Cr], where the square brackets symbolize the concentrations of the given metabolites (in this example, choline and creatine). For brevity, this nomenclature will be adopted for the most part in the present analysis, with the understanding that the clause: “the ratio of two given metabolites” actually means “the ratio of these metabolite concentrations”.

The OVID MEDLINE data base was first used including search terms as key words plus the "explode"[3] option, with the strategy: (magnetic resonance spectroscopy) AND (radiation therapy) AND (brain tumor). The limits were papers in English and studies on human patients. This OVID MEDLINE search yielded 111 abstracts, each of which was reviewed. Of these, 42 potentially eligible papers were identified. A search replication via the PUBMED data base yielded 228 abstracts, from which 5 more potentially eligible papers were identified that were not found through the MEDLINE search. These searches were performed through June 2011. Personal files were also scrutinized. Altogether, 46 abstracts were identified as potentially eligible for the present study. The full-length papers were analyzed for these 46 abstracts to determine whether they fulfilled the following criteria:

(1) Empirical clinical study of patients treated by RT for primary malignant brain tumor with a new lesion detected after RT,
(2) Use of in vivo proton MRS or MRSI data to evaluate the new lesion, and
(3) Clinical and MRS data provided for individual patients.

After this scrutiny, 6 articles were retained for further analysis in the present work.

2.2 Data management

The data from each individual patient were entered into a single data set for statistical analysis. These data included demographic information about the patients, grade of the primary brain tumor according to the World Health Organization classification scheme [18], details about the MRS recording conditions, such as magnetic field strength B_0 and echo time (TE), reported numerical values for various metabolite ratios, as well as the clinical outcome or observation (recurrent tumor versus radiation necrosis).

2.3 Statistical analysis

"Statistica" software was used for all the presented statistical analyses. The data were analyzed with respect to recurrent tumor versus radiation necrosis as the outcome variable, unless otherwise stated. Mean, standard deviation σ and range were determined for continuous and semi-continuous[4] variables (patient age, magnetic field strength, echo time, and the metabolite ratios). The number of patients and their percentages were assessed for the dichotomous covariates (i.e. gender and high-grade versus lower-grade primary tumor). Missing data were noted throughout.

Differences between recurrent tumor versus radiation necrosis were first assessed with respect to continuous and semi-continuous variables by the Mann-Whitney U test, where $U = n_1 n_2 + n_1(n_1+1)/(2-R_1)$ with R_1 being the sum of ranks of Group

[3] "Explode" is an option within OVID MEDLINE, which provides the broadest possible inclusion of studies.

[4] Semi-continuous variables are those in which there are three or more numerical values that reflect quantity or intensity. In contrast, the numerical values of dichotomous variables (often termed "categorical" variables) are often assigned arbitrarily. Thus, these latter numerical values usually do not necessarily reflect quantity or intensity.

1 and n_1 and n_2 being the number of patients in Group 1 and Group 2 [23]. In the present analysis, recurrent tumor is treated as Group 1.

Pearson χ^2 tests were used to evaluate differences between tumor recurrence and radiation necrosis with respect to the dichotomous independent variables. The χ^2 were computed as follows:

$$\chi^2 = \sum_{i=1}^{r} \sum_{j=1}^{k} \frac{(\mathrm{O}_{ij} - \mathrm{M}_{ij})^2}{\mathrm{M}_{ij}}, \tag{1}$$

where r is the number of rows and k is the number of columns, O_{ij} is the observed number of cases categorized in the ith row of the jth column of matrix $\mathbf{O} = \{\mathrm{O}_{ij}\}$ and M_{ij} is the number of cases predicted by the model under the null hypothesis to be categorized in the ith row of the jth column of matrix $\mathbf{M} = \{\mathrm{M}_{ij}\}$.[5]

Associations with and between metabolite ratios were assessed using Spearman's correlation:

$$\rho = 1 - \frac{6 \sum_{i=1}^{N} d_i^2}{N^3 - N}, \tag{2}$$

with $d_i = X_i - Y_i$, where X_i and Y_i are the ranks of variables X and Y, respectively for patient "i" and N is the total number of patients. The possible range of ρ is from $+1$ (maximum positive correlation) to -1 (maximum inverse correlation) [23]. This correlation analysis was performed to help identify covariates for which adjustment should be made, as well as for deciding whether the subsequent use of the logistic regression model could include more than one metabolite ratio as an independent variable [24].

The positive and negative predictive values and overall accuracy[6] of the metabolite ratios for identifying recurrent tumor as opposed to radiation necrosis were assessed using logistic regression analysis. Logistic regression (which is also called the logit model) is a procedure which, via a rational function, estimates a model which describes the relationship between the independent and dependent variables, when the dependent variable (y) is binary [25]. A binary or a Bernoulli variable is a discrete variable which can take only the two values 0 or 1. In the present analysis, these values refer to the outcome variable, whether the individual patient was diagnosed as having radiation necrosis or tumor recurrence, respectively. Specifically, logistic regression transforms y into a continuous variable within the bounds from 0 to 1, regardless of the values of the independent variables (x):

[5] In the statistical literature the term "expected" is customarily used instead of the term "predicted from the model". The latter is more appropriate since it explicitly refers to theoretical modelling. We therefore use the term "predicted from the model" throughout.

[6] Positive predictive value = (true positive results) / (true positive results + false positive results).
Negative predictive value = (true negative results) /(true negative results + false negative results).
Overall accuracy = (true positive results + true negative results) / (all results), where
all results = true positive results + false positive results + true negative results + false negative results.

$$y = \frac{e^L}{1 + e^L}, \quad L \equiv \alpha + \sum_{k=1}^{n} \beta_k x_k = \alpha + (\beta_1 x_1 + \cdots + \beta_n x_n). \tag{3}$$

Here, α is a constant, and the coefficients $\{\beta_k\}$ $(1 \leq k \leq n)$ are the predictor parameters, whereas L is the logistic or logit transformation,

$$L = \ln \frac{y}{1 - y}. \tag{4}$$

By means of logistic regression, it is possible to predict the category of outcome for individual cases using the most parsimonious model (the least number of parameters). In particular, Eq. (3) maps L into y which has the meaning of probability P, and for this reason we have $(0 \leq y \leq 1)$. For example, if $L = 3.425$, it follows that $y \equiv P = 0.0315$. In the present analysis, the dependent variable y is the outcome of the modelled prediction (recurrent tumor versus radiation necrosis) and the set of independent variables $x = \{x_1, \ldots, x_n\}$ represents the input data given by the metabolite ratio or ratios assessed alone or together with the covariates for which adjustment is being made. The modelled prediction y, as a continuous variable $(0 \leq y \leq 1)$, is rounded in the end to express it as the corresponding Bernoulli variable 0 and 1 for the purpose of a direct comparison with the observations.

As mentioned, in practice, the so-called cutpoint values for metabolite ratios have often been used. These cutpoints represent certain fixed values of metabolite concentration ratios. The value of the given metabolite concentration ratio as an independent variable in the form of a rational number is thereby converted into a Bernoulli variable 0 or 1. For this purpose, the standard definition of the Heaviside step function is used for the independent variable x:

$$x = \begin{cases} 0, & x < x_{\text{cut}} \\ 1, & x \geq x_{\text{cut}} \end{cases}.$$

For example, for $x =$ [Cho]/[Cr] we made three additional sets of logistic regressions using $x_{\text{cut}} = 1.5$, 2.0 and 2.5. Clearly, this procedure modifies the raw input data and it is not expected that any improvement in the diagnostic accuracy will be obtained. This will be seen by comparing the results from logistic regression analysis when the metabolite ratios are used as the raw data and when they are converted into the Bernoulli variables, as described above for the three cutpoints.

The meaning of the logit function L from Eq. (3) can be interpreted in terms of the risk ratio (RR):

$$\text{RR} \equiv \frac{P_1}{P_0}, \quad P_1 = \Pr(y = 1 \mid x), \quad P_0 = \Pr(y = 0 \mid x).$$

Here, $\Pr(y = 1 \mid x)$ is the probability of the prediction y being 1. Conservation of probability implies

$$\Pr(y = 0 \mid x) = 1 - \Pr(y = 1 \mid x).$$

Setting:

$$P_1 = \frac{e^L}{1 + e^L}$$

and using the complementary probability $P_0 = 1 - P_1$, it follows:

$$P_0 = \frac{1}{1 + e^L}.$$

This gives the risk ratio as:

$$\mathrm{RR} = e^L$$

or equivalently, by taking the natural logarithm:

$$L = \ln(\mathrm{RR}) = \ln \frac{P_1}{P_0} = \ln \frac{\Pr(y = 1 \mid x)}{\Pr(y = 0 \mid x)}.$$

Given that the denominator $\Pr(y = 0 \mid x)$ is equal to $1 - \Pr(y = 1 \mid x)$, we can rewrite the preceding expression as $L = \ln\{\Pr(y = 1 \mid x)/[1 - \Pr(y = 1 \mid x)]\}$, or shorter, $L = \ln\{y/(1-y)\}$ which coincides with Eq. (3). This derivation shows that the logit transformation L, as a linear combination of independent variables $\{x_1, \ldots, x_n\}$, augmented by the constant α, via $L = \alpha + (\beta_1 x_1 + \cdots + \beta_n x_n)$ represents the natural logarithm of the risk ratio. A similar analysis can also be applied to derive a link between the logit function L and the odds ratio (OR) defined by:

$$\mathrm{OR} = [P_1/(1 - P_1)]/[P_0/(1 - P_0)].$$

In the numerous studies from which the 6 articles qualified to be included in the present analysis, assessment of the predictive power of a given ratio of metabolite concentrations with regard to radiation necrosis versus tumor recurrence, was mainly done by merely reporting the so-called p values. The p value is the probability that a given finding occurs solely by chance, i.e. at random. We presently aim to go beyond these rudimentary estimates by employing a logistic regression model (3) for meta-analysis of the available data. The added value of this step is in a more comprehensive, integrative assessment of the predictive power of metabolite concentration ratios. This is achieved by obtaining the continuous as well as the Bernoulli dependent variable y for the sought probability that a given metabolite concentration ratio x_1 has the said predictive power in a statistically significant way but also for a given patient, with and without adjustment for covariates as additional independent variables that could influence the distribution of y.

2.3.1 The algorithm for the logistic regression analysis

In the simplest case when the vector $x = \{x_1, \ldots, x_n\}$ has a single variable x_1, we have $y = 1/\{1+\exp(-\alpha-\beta x)\}$ where $x = x_1$ and $\beta = \beta_1$. Such y is the univariate function

of one independent variable x. In our application, we can set e.g. x = [Cho]/[Cr] and the ensuing y will be said to be unadjusted for any of the possible confounding factors, e.g. TE, B_0, grade of the primary tumor. The veracity of such an unadjusted predictor for y should be subsequently checked against the possible role of these confounding factors, as well shall do. As stated, this is done by treating these confounding factors as covariates. In principle, we could have a bivariate model $y = 1/\{1 + \exp(-\alpha - \beta_1 x_1 - \beta_2 x_2)\}$, a trivariate model $y = 1/\{1 + \exp(-\alpha - \beta_1 x_1 - \beta_2 x_2 - \beta_3 x_3)\}$ or a four-variate model $y = 1/\{1 + \exp(-\alpha - \beta_1 x_1 - \beta_2 x_2 - \beta_3 x_3 - \beta_4 x_4)\}$, where for example x_1 = [Cho]/[Cr], x_2 = TE, $x_3 = B_0$ and x_4 = grade of the primary tumor, etc. The resulting y would then be said to be adjusted for one covariate at a time (bivariate logistic regression) or for two covariates simultaneously (trivariate logistic regression) or for three covariates simultaneously (four-variate logistic regression). In any of these cases, the algorithm is used for only one metabolite ratio at a time, (x_1 = [Cho]/[Cr] in this example). The same algorithm will be separately applied for other ratios [A]/[B] with the selected concentrations of any two other metabolites A and B.

It is also possible to extend this algorithm to encompass a more complex interplay with simultaneous inclusion of two or more metabolite ratios. For example, one can obtain y with the two simultaneously treated variables (x_1 = [Cho]/[Cr]) and (x_2 = [NAA]/[Cr]) with an unadjusted bivariate prediction: $y = 1/\{1 + \exp(-\alpha - \beta_1 x_1 - \beta_2 x_2)\}$ or the adjusted five variate prediction: $y = 1/\{1 + \exp(-\alpha - \beta_1 x_1 - \beta_2 x_2 - \beta_3 x_3 - \beta_4 x_4 - \beta_5 x_5)\}$, where x_3 = TE, $x_4 = B_0$ and x_5 = grade of the primary tumor. Some of these variants will be used in the next section. Whichever version is employed, $x = \{x_1, \ldots, x_n\}$ is the set of given entry data (metabolite concentration ratios, TE, B_0 and grade of the primary tumor). Another set of known input data is $Y = \{y_1, \ldots, y_N\}$ where N is the total number of patients. Here, the dependent variable $y_i^{(O)}$ is the observation for patient "i" ($1 \le i \le N$). Each $y_i^{(O)}$ is a dichotomous variable which has two possible integer values "0" and "1". For definiteness, these "0" and "1" values for every $y_i^{(O)}$ are associated with the clinical observations of "radiation necrosis" and post-RT "tumor recurrence", respectively. The goal of the presently applied regression analysis is to determine how reliable is a given metabolite concentration ratio in obtaining agreement between the model (3), i.e. prediction $y_i^{(M)}$ and observation $y_i^{(O)}$, where:

$$y_i^{(M)} = \frac{e^{L_i}}{1 + e^{L_i}}, \quad L_i = \alpha_i + \sum_{k=1}^{n} \beta_{k,i} x_{k,i}.$$

Here, subscript "i" is introduced in L, α, β and $\{x_1, \ldots, x_n\}$ to make reference to patient "i". To compute $y_i^{(M)}$, the unknown parameters α_i and $\{\beta_i\}(1 \le k \le n)$ need to be obtained first. These are estimated by minimizing the errors between $y_i^{(O)}$ and $y_i^{(M)}$. To this end, the iterative least square minimization is employed:

$$\min \sum_{k=1}^{n} w_i [y_i^{(O)} - y_i^{(M)}]^2, \quad \Rightarrow \alpha_i, \quad \{\beta_{k,i}\}(1 \le k \le n),$$

where w_i are certain judiciously chosen weight factors that can influence the efficiency of estimation of the parameters α_i and $\{\beta_{k,i}\}$. Once all the parameters α_i and $\{\beta_i\}$ become available, L_i can be calculated for the given input data $\{x_{k,i}\}$ and this finally yields the sought prediction $y_i^{(\mathrm{M})}$ of $y_i^{(\mathrm{O})}$ for each patient "i" ($1 \leq i \leq N$). The result $y_i^{(\mathrm{M})}$ is necessarily a real number with decimals, i.e. a non-integer. Moreover, being a probability, $y_i^{(\mathrm{M})}$ belong to the interval [0,1]. On the other hand, as stated, $y_i^{(\mathrm{O})}$ takes exclusively only two integer values with $y_i^{(\mathrm{O})} = 0$ or $y_i^{(\mathrm{O})} = 1$ for necrosis or recurrence, respectively. Thus, to compare $y_i^{(\mathrm{M})}$ with $y_i^{(\mathrm{O})}$, the real numbers $y_i^{(\mathrm{M})}$ should be converted to the Bernoulli variables 0 and 1 using the Heaviside step function:

$$y_i^{(\mathrm{M})} = \begin{cases} 0, & y_i < 0.5 \\ 1, & y_i \geq 0.5 \end{cases}.$$

These dichotomized predictions $y_i^{(\mathrm{M})}$ with their values 0 and 1 are compared to the observed $y_i^{(\mathrm{O})}$ integers, in order to give the answers for each patient as to the reliability of the metabolite concentration ratios in predicting the outcome "radiation necrosis" versus "tumor recurrence".

3 Results

As stated, six articles fulfilled the criteria for inclusion in the present study and these are the works of the groups of Kamada [7], Matsusue [8], Nakajima [9], Weybright [15], Zeng [19] and Smith [20]. Table 1 provides a brief summary of the clinical aspects and design of these 6 studies, together with salient information about the reported MRS data.

Altogether, these 6 papers provide quantitative MRS data on sixty-three patients with recurrent brain tumors and on thirty-eight patients with radiation necrosis. The results of our analysis comparing these two groups are presented in Table 2. It is seen that the two groups are similar with regard to age and gender, but there are substantial missing data for both of these variables. The primary brain tumors were high grade (Grade III or IV) in altogether sixty-seven (66.3 %) of the patients. Significantly more patients with radiation necrosis after RT had a high-grade primary brain tumor. The B_0 of the MR scanner and TE were similar for the two patient groups. Complete data on all 101 patients were available only for choline to creatine ratios. Ratios of choline to creatine and of choline to NAA were significantly higher among the patients with recurrent tumors post-RT, whereas NAA to creatine ratios were significantly lower. The lactate to choline ratios were available for less than one-third of the patients and these ratios were significantly higher among the patients with radiation necrosis. The lactate to creatine ratios were available only for six patients with recurrent tumor, having a mean $\pm\, \sigma$ value of 1.65 ± 0.51, ranging from 0.81 to 2.23 and for three patients with radiation necrosis (mean $\pm\, \sigma = 8.55 \pm 4.97$, range 3.56–13.5).

A significant direct correlation was observed between choline to creatine ratios ($x_1 =$ [Cho]/[Cr]) and echo time ($x_2 =$ TE). Between these two variables, $\rho = 0.26$

Table 1 Summary of MRS studies included in the meta-analysis on recurrent tumor versus radiation necrosis post-RT for primary malignant brain tumors

1st author, publication year [reference #] center, city, country	Clinical data/study design	RT	B_0(T) and TE	Endpoint	MRS criteria	Comments
Kamada, 1997 [7] Hokkaido University, Sapporo, Japan	10 patients with 1° gliomas and 1 patient with maxillary cancer, post-RT Cross-sectional comparison of the patients with recurrent patient and RN Clinical follow-up of all patients reported	38-65 Gy	1.5T TE = 270 ms	Histologically-confirmed recurrent glioma (6 patients) versus RN (5 patients, biopsy-proven in 4 patients)	VOI selected to contain the bulk of the lesion but avoid overlapping with bone marrow and surrounding brain tissue The following metabolite ratios reported: Cho/Cr, NAA/Cr, Lac/Cr and Lac/Cho	The patient with maxillary cancer is excluded from the present analysis Data on metabolite ratios provided for only 3 of the 5 patients with RN
Weybright, 2004 [15] University of Michigan, Ann Arbor, USA	8 patients Tx for malignant posterior fossa or brainstem tumor (gliomas, medulloblastoma or astrocytoma + one patient with acute myeloid leukemia) with new CE lesion 7 of these patients received RT (4 also received surgery and 6 received Chemotx) Prospective: follow-up from 8 to 28 months	Details not described	1.5T TE = 144 ms	Recurrent tumor assessed by imaging/clinical follow-up (5 patients) vs. Tx.-related changes, absence of tumor confirmed by biopsy (3 patients)	MRSI: voxels included the CE lesion as well as normal-appearing cerebellum (6 patients) MRS: voxel in the CE lesion (2 patients) The following metabolite ratios reported in the CE lesion: NAA/Cr, Cho/Cr, Cho/NAA	One patient who did not receive RT and one patient with acute myeloid leukemia and CNS involvement are excluded from the present analysis Data on metabolite ratios not provided for one other patient

Table 1 continued

1st author, publication year [reference #] center, city, country	Clinical data/study design	RT	B_0(T) and TE	Endpoint	MRS criteria	Comments
Zeng, 2007 [19] Qilu Hospital of Shandong University, Jinan, China	28 patients with high-grade gliomas, new CE lesion in the vicinity of the original tumor Prospective: follow-up varied according to clinical course	All patients had undergone "full course of conventional fractionated RT after surgery"	3T TE = 144 ms	RT injury (9 patients) versus recurrent tumor (17 patients) Clinical and imaging follow-up or histopathology	MRSI: over the CE lesion The following metabolite ratios reported in the CE lesion: NAA/Cr, Cho/Cr, Cho/NAA	No individual demographic data presented Individual MR data presented for 26 of the 28 patients
Nakajima, 2009 [9] Tohoku University, Sendai, Japan	18 patients with histologically-confirmed glioma who after RT+ Chemotx had a subsequent lesion on MRI suspected to be RN versus tumor recurrence from CE and T_2 Retrospective analysis: of patients who had been followed every 2–3 M, up to 158 M	Described only in selected cases presentations	1.5T TE=272 ms	Recurrent tumor (7 patients) vs RN (11 patients) Confirmed by surgical resection or biopsy (14 patients) or by imaging + clinical follow (4 patients)	MRS: of representative part of the CE lesion The following metabolite ratios reported in the CE lesion: Cho/Cr, Lac/Cho	Data on metabolite ratios not provided for two patients

Table 1 continued

1st author, publication year [reference #] center, city, country	Clinical data/study design	RT	B_0(T) and TE	Endpoint	MRS criteria	Comments
Smith, 2009 [20] University of Michigan, Ann Arbor, USA	33 patients with primary brain tumor grade II-IV histopathologically proven, previous RT with or without Chemotx and a new CE-lesion, subsequently Retrospective	54–70 Gy ("conventional fractionated")	1.5T TE = 144 ms	Recurrent tumor (20 patients) versus RN (13 patients) Imaging follow-up or histopathology	MRSI: chose 1 voxel with highest values for all NAA/Cr; Cho/Cr; Cho/NAA ratios Lac, lipid also assessed	
Matsusue, 2010 [8] University of Washington, Seattle, USA	15 patients with glioma Tx with subtotal or gross total resection plus RT, in some cases Chemotx who had developed a new CE lesion or ↑ T_2 region, post-RT Retrospective review	EBRT in all patients (54–72 Gy, some un-specified) + SRS (5 patients)	3T TE = 36–288 ms	Recurrent tumor (10 patients) versus RN (5 patients) Histological confirmation (3 patients) or clinical + imaging (12 patients)	MRSI performed unless poor quality to due magnetic field inhomogeneities, then MRS Voxel with highest Cho/Cr, Cho/NAA chosen	Individual MR data presented for 13 of the 15 patients

CE contrast enhancement, *Chemotx* chemotherapy, *Cho* choline, *Cr* creatine, *CRT* conformal radiation therapy, *EBRT* external beam radiotherapy, *Gy* gray, *Lac* lactate, *M* months, *MRS* magnetic resonance spectroscopy, *MRSI* magnetic resonance spectroscopic imaging, *ms* milliseconds, *NAA* N-acetyl aspartate, *RN* radiation necrosis, *RT* radiation therapy, *SRS* stereotactic radiosurgery, *T* tesla, *TE* echo time, *Tx* therapy or treated, *U* university, *VOI* voxel of interest, *vs* versus

Table 2 Univariate analysis comparing recurrent tumor versus radiation necrosis

	Recurrent tumor $N = 63$	Significance	Radiation necrosis $N = 38$
	Number (%)		Number (%)
Patient gender			
Male	22 (55)		16 (61.5)
Female	18 (45)		10 (38.5)
Missing	23		12
High grade primary brain tumor			
Yes	37 (58.7)	*	30 (78.9)
No	26 (41.3)		8 (21.1)
	Mean ± SD (range)		Mean ± SD (range)
Patient age	40.1 ± 16.2 (4–66)		39.8 ± 18.1 (7–67)
Missing	17		9
Magnetic field strength	2.14 ± 0.75 (1.5–3.0)		1.97 ± 0.71 (1.5–3.0)
Echo time	168 ± 65 (36–288)		181 ± 64 (37–272)
Metabolite ratios:			
Choline to creatine	2.54 ± 0.84 (1.29–4.39)	***ξ	1.72 ± 0.62 (0.64–3.62)
Choline to N-acetyl aspartate	2.92 ± 1.53 (0.72–6.47)	***	1.44 ± 0.46 (0.56–2.40)
Missing	13		12
N-acetyl aspartate to creatine	0.83 ± 0.28 (0.00–1.38)	*	1.06 ± 0.50 (0.00–2.60)
Missing	18		12
Lac/Cho	0.59 ± 0.22 (0.24–1.01)	**ξ	3.07 ± 2.91 (1.09–10.8)
Missing	50		26

Comparisons for the categorical variables assessed by Pearson χ^2 tests
Means are compared with two-sample t tests, unless indicated as ξ for Mann-Whitney test
*, ** and *** denote $p < 0.05$, $p < 0.01$ and $p < 0.001$, respectively; all significance levels 2 sided. *SD* standard deviation
The data for a given variable are complete unless otherwise indicated

and $p = 0.008$, where, as noted earlier, p is the probability that the finding occurred purely by chance, i.e. at random. An inverse correlation of borderline statistical significance ($\rho = -0.21$, $p = 0.075$) was also found between choline to NAA ratios ($x_1 = [\text{Cho}]/[\text{NAA}]$) and the value in tesla (T) of the magnetic field strength ($x_2 = \text{B}_0$).

The ratios of choline to creatine and of NAA to creatine showed significant inverse correlation ($\rho = -0.31$, $p = 0.009$) at a level which would permit their inclusion in the same logistic regression model [24]. On the other hand, the ratios of choline to creatine and choline to NAA were very highly correlated ($\rho = 0.77$, $p = 0.00000$), such that it would not be appropriate to include these two ratios in the same logistic regression model [24]. Because of the large amount of missing data for ratios of lactate to choline, combined regression analysis with the other metabolite ratios would severely compromise statistical power and was therefore not performed. It should also be noted that all the lactate to choline and lactate to creatine ratios were reported for echo times of 270 or 272 ms.

Table 3 Positive and negative predictive values and overall accuracy of metabolite ratios as indicators of recurrent brain tumor after radiation therapy as opposed to radiation necrosis

Unadjusted analysis Observed result				Adjusted for high-grade primary tumor, TE and B_0 Observed result			
Predicted result	RTu	RN	% correct	Predicted result	RTu	RN	% correct
Choline to creatine ratio (Cho/Cr)							
RTu	49	11	81.7 (PPV)	RTu	55	10	84.6 (PPV)
RN	14	27	65.9 (NPV)	RN	8	28	77.8 (NPV)
	63	38	Overall accuracy = 75.2		63	38	Overall accuracy = 82.2
$\chi^2 = 26.2$, $p = 0.0000003$				$\chi^2 = 41.3$, $p = 0.000000$			
Choline to N-acetyl aspartate ratio (Cho/NAA)							
RTu	41	11	78.9 (PPV)	RTu	44	6	88.0 (PPV)
RN	9	15	62.5 (NPV)	RN	6	20	76.9 (NPV)
	50	26	Overall accuracy = 73.7		50	26	Overall accuracy = 84.2
$\chi^2 = 28.2$, $p = 0.0000001$				$\chi^2 = 38.4$, $p = 0.0000001$			
N-Acetyl aspartate to creatine ratio (NAA/Cr)							
RTu	43	19	69.4 (PPV)	RTu	40	15	72.7 (PPV)
RN	2	7	77.8 (NPV)	RN	5	11	68.8 (NPV)
	45	26	Overall accuracy = 70.4		45	26	Overall accuracy = 71.8
$\chi^2 = 6.6$, $p = 0.01$				$\chi^2 = 13.2$, $p = 0.01$			
Lactate to choline ratio (Lac/Cho)							
RTu	12	0	100 (PPV)	RTu	12	0	100 (PPV)
RN	0	13	100 (NPV)	RN	0	13	100 (NPV)
	12	13	Overall accuracy = 100		12	13	Overall accuracy = 100
$\chi^2 = 33.6$, $p = 0.000000$				$\chi^2 = 34.6$, $p = 0.0000006$			
Choline to creatine ratio (Cho/Cr) and N-acetyl aspartate to creatine ratio (NAA/Cr)							
RTu	37	4	90.2 (PPV)	RTu	39	4	90.7 (PPV)
RN	8	22	73.3 (NPV)	RN	6	22	78.6 (NPV)
	45	26	Overall accuracy = 83.1		45	26	Overall accuracy = 85.9
$\chi^2 = 35.6$, $p = 0.000000$				$\chi^2 = 41.8$, $p = 0.0000001$			

Computations performed via logistic regression analysis
NPV negative predictive value, *PPV* positive predictive value, *RTu* recurrent tumor, *RN* radiation necrosis, *TE* echo time

Table 3 presents the logistic regression analysis with the various metabolite ratios as independent variables. For each logistic regression, we present the number of correctly predicted cases of recurrent tumor and of radiation necrosis, the positive and negative

Table 4 Positive and negative predictive values and overall accuracy of various cutpoints for choline to creatine ratios (Cho/Cr) as indicators of recurrent brain tumor after radiation therapy as opposed to radiation necrosis

Unadjusted analysis Observed result				Adjusted for high-grade primary tumor, TE and B_0 Observed result			
Predicted result	RTu	RN	% correct	Predicted result	RTu	RN	% correct
Choline to creatine ratio (Cho/Cr) ≥1.5							
RTu	59	24	71.1 (PPV)	RTu	60	25	70.6 (PPV)
RN	4	14	77.8 (NPV)	RN	3	13	81.3 (NPV)
	63	38	Overall accuracy = 72.3		63	38	Overall accuracy = 72.3
$\chi^2 = 14.9$, $p = 0.0001$				$\chi^2 = 23.4$, $p = 0.0001$			
Choline to creatine ratio (Cho/Cr) ≥2							
RTu	40	8	83.3 (PPV)	RTu	48	14	77.4 (PPV)
RN	23	30	56.6 (NPV)	RN	15	24	61.5 (NPV)
	63	38	Overall accuracy = 69.3		63	38	Overall accuracy = 71.3
$\chi^2 = 18.0$, $p = 0.00002$				$\chi^2 = 31.7$, $p = 0.000002$			
Choline to creatine ratio (Cho/Cr) ≥2.5							
RTu	32	4	88.9 (PPV)	RTu	55	20	73.3 (PPV)
RN	31	34	52.3 (NPV)	RN	8	18	69.2 (NPV)
	63	38	Overall accuracy = 65.3		63	38	Overall accuracy = 72.3
$\chi^2 = 18.7$, $p = 0.00002$				$\chi^2 = 30.0$, $p = 0.000005$			

Computations performed via logistic regression analysis
NPV negative predictive value, *PPV* positive predictive value, *RTu* recurrent tumor, *RN* radiation necrosis, *TE* echo time

predictive values, and the overall accuracy of the regression model. The left panels of Table 3 show the unadjusted logistic regression analysis, whereas the right panels are adjusted for high versus lower grade of the primary tumor, TE and B_0. The χ^2 values of each logistic regression analysis and the p values are also presented. Higher choline to creatine and choline to NAA ratios were associated with a significantly greater likelihood of recurrent tumor, as opposed to radiation necrosis. This was found both with and without adjustment for tumor grade, TE and B_0. Higher NAA to creatine and lactate to choline ratios were associated with a significantly greater likelihood of radiation necrosis as opposed to recurrent tumor, both with and without adjustment for tumor grade, TE and B_0. It was only the lactate to choline ratio which yielded 100 % overall accuracy of all the cases for which data were available. Consistent with this finding is that there were no overlaps in the ranges of lactate to choline ratios for recurrent tumor versus radiation necrosis. However, as noted, data were available for less than one-third of the patients. The adjusted logistic regression model that included both the ratios of choline to creatine and of NAA to creatine improved the overall accuracy compared to either metabolite ratio alone.

Table 5 Positive and negative predictive values of various cutpoints for choline to NAA ratios (Cho/NAA) as indicators of recurrent brain tumor after radiation therapy as opposed to radiation necrosis

Unadjusted analysis Observed result				Adjusted for high-grade primary tumor, TE and B_0 Observed result			
Predicted result	RTu	RN	% correct	Predicted result	RTu	RN	% correct
			Choline to NAA ratio ≥1.5				
RTu	42	11	79.3 (PPV)	RTu	42	7	85.7 (PPV)
RN	8	15	65.2 (NPV)	RN	8	19	70.4 (NPV)
	50	26	Overall accuracy = 75		50	26	Overall accuracy = 80.3
$\chi^2 = 13.8$, $p = 0.0002$				$\chi^2 = 26.7$, $p = 0.00002$			
			Choline to NAA ratio ≥2				
RTu	30	3	90.9 (PPV)	RTu	46	14	76.7 (PPV)
RN	20	23	53.5 (NPV)	RN	4	12	75 (NPV)
	50	26	Overall accuracy = 69.7		50	26	Overall accuracy = 76.3
$\chi^2 = 18.1$, $p = 0.00002$				$\chi^2 = 27.6$, $p = 0.00002$			
			Choline to NAA ratio ≥2.5				
RTu	25	0	100 (PPV)	RTu	46	16	74.2 (PPV)
RN	25	26	51 (NPV)	RN	4	10	71.4 (NPV)
	50	26	Overall accuracy = 67.1		50	26	Overall accuracy = 73.7
$\chi^2 = 27$, $p = 0.0000002$				$\chi^2 = 32.8$, $p = 0.000001$			

Computations performed via logistic regression analysis
NPV negative predictive value, *PPV* positive predictive value, *RTu* recurrent tumor, *RN* radiation necrosis, *TE* echo time

We examined three cutpoints for choline to creatine (Table 4) and choline to NAA ratios (Table 5) and these were: ≥1.5, ≥2 and ≥2.5. Ratios greater than or equal to each of these cutpoints were associated with a significantly increased likelihood of recurrent tumor. Nevertheless, none of these cutpoints provided substantially better prediction than did the overall choline to creatine or choline to NAA ratios.

Figure 1 presents the observed $y_i^{(O)}$ versus the predicted $y_i^{(M)}$ outcome for each of the one hundred and one patients $i\,(1 \le i \le N, N = 101)$, based upon the unadjusted and adjusted choline to creatine ratios. The predictions $y_i^{(M)}$ are from the logistic regression model (3), whereas the observations $y_i^{(O)}$ are the input data as binary variables 0 and 1. In the top panel (a) the predictions $y_i^{(M)}$ are shown as continuous variables. Here, one can see whether or not the prediction was correct for each individual patient, whether or not adjusting for high-grade tumor, TE and B_0 improved the prediction and how far the predictions deviated from the observed outcome. The observed values are compared with the unadjusted rounded predictions in the middle panel (b), and in the bottom panel (c) with the adjusted rounded predictions. We chose the choline to

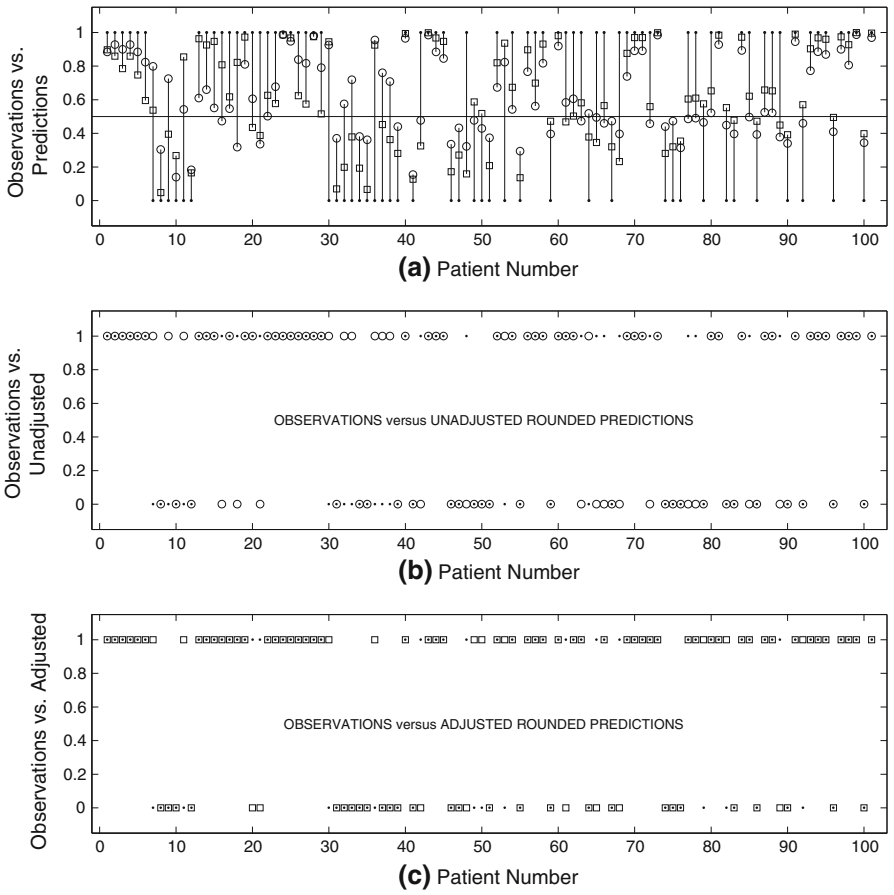

Fig. 1 The observed versus predicted outcome for each of the one hundred and one patients, based upon the choline to creatine ratio using logistic regression. The abscissae indicate the patient number and the ordinates compare the predicted with the observed outcome (*full small dots*) where the value 1 denotes recurrent tumor, whereas 0 is radiation necrosis. *Open circles* represent the unadjusted prediction and *open squares* indicate the predicted value with adjustment for echo time, magnetic field strength and grade of the primary brain tumor. In the top panel (**a**) the predictions are shown as computed, continuous variables. The *middle horizontal line* on panel (**a**) is drawn at the ordinate value of 0.5 to facilitate a visual inspection of the subsequent rounding of the continuous predictions on panels (**b**) and (**c**). The *vertical lines* for each patient number are drawn through all three displayed data points to guide the eye while comparing the observations with the unadjusted and adjusted predictions. The observed values are compared with the unadjusted rounded predictions in the middle panel (**b**), and in the bottom panel (**c**) with the adjusted rounded predictions (rounding to 0 or 1, see the text)

creatine ratio for this graphic representation since this was the only ratio for which complete data were available for all the patients included in the meta-analysis.

In eleven of the one hundred and one patients (10.9), the unadjusted and adjusted predictions were both wrong. These included six individual patients with recurrent tumors for whom both the unadjusted as well as the adjusted model predicted radiation necrosis. Conversely, for five patients with radiation necrosis both the unadjusted and adjusted models predicted recurrent tumor.

Although the adjusted model improved the positive and negative predictive value as well as overall accuracy of the choline to creatine ratio (Table 3), it can be observed from panel (a) of Fig. 1 that on the individual level, this was not the case for the majority of patients. Namely, in sixty-three of the patients (62.3 %), the adjusted model provided estimates that were farther away from observed value than was the unadjusted value.

4 Discussion: with reference to an alternative mathematical approach to quantification of MRS data

4.1 Use of ratios of metabolite concentrations for clinical decision-making in neuro-oncology

All the computed metabolite concentration ratios for which substantial data were available provided significant distinction between recurrent tumor and radiation necrosis after radiation therapy. On the other hand, the results of the presented meta-analysis indicate that none of the analyzed metabolite ratios qualify as most reliable for differentiating recurrent brain tumor post-RT from radiation necrosis. Furthermore, this meta-analysis shows that no cutpoint for the choline to creatine or choline to NAA ratios optimally distinguishes these two clinical entities. With higher cutpoints in the unadjusted analyses, the positive predictive value improved, but the negative predictive value worsened. In other words, more recurrent tumors would be missed with higher metabolite ratio cutpoints.

It is known that metabolite ratios can be affected by echo time [26,27] and by magnetic field strength [28]. Concordantly, we found that the choline to creatine ratio was significantly correlated with echo time, and a borderline inverse correlation was observed between magnetic field strength and choline to NAA ratio. Adjustments for echo time and magnetic field strength did provide some improvement in the overall accuracy, i.e. the correct number of clinical outcomes predicted by the metabolite ratios. Nevertheless, such adjustments did not help identify optimal cutpoints. Moreover, as illustrated in Fig. 1, on the level of individual patients, adjusting for TE, B_0 as well as grade of the primary tumor did not improve the closeness with which the choline to creatine ratios predicted the actual clinical outcome. In over ten percent of cases, the clinical outcome was incorrectly predicted both by the unadjusted as well as the adjusted choline to creatine ratios.

Metabolite ratios (most often choline to creatine and choline to NAA) have been used quite extensively to identify primary brain tumors. Comparing MRI-localized proton spin density spectra from healthy volunteers with the MR spectra from the tumor bed of fifty-one patients with high-grade gliomas, Tarnawski et al. [29] reported significantly higher choline to creatine and choline to NAA ratios in the latter. Lin et al. [30] found that the choline to creatine ratio assessed at short echo-time was significantly higher among forty-nine patients with biopsy-proven brain tumors compared with fourteen healthy controls. The mean choline to NAA ratios from brain regions without tumor were 1.7 ± 1.2 versus 5.3 ± 2.1 to 6.8 ± 3.7 in gliomas, depending upon the grade, in a study by McKnight et al. [31] in which all findings were confirmed histopathologically. Hourani et al. [32] found that an NAA to choline ratio ≤ 0.61

together with a relative cerebral blood flow ≥ 1.5 distinguished sixty-nine patients with primary brain tumors of various grades from thirty-six patients with diverse non-cancerous brain lesions, with a sensitivity of 72 % and specificity of 92 %. Choline to NAA ratios >1.9 reportedly helped neuroradiologists to distinguish malignant from pseudo-tumorous lesions in a study of eighty-four patients with solid brain masses [33].

In contrast with these positive findings for identifying brain tumors using metabolite ratios, in a study by Smith et al. [34], choline to creatine ratios among five healthy volunteers ranged from 1.54 to 2.14 (mean $\pm\, \sigma = 1.8 \pm 0.1$), the choline to creatine ratio in non-neoplastic brain stem lesions (fungal infection, gliosis, inflammation, multiple sclerosis, and necrosis) ranged from 0 to 2.6 (mean $\pm\, \sigma = 1.4 \pm 0.2$). On the other hand, among patients with solitary neoplastic brain stem lesions (astrocytoma, ganglioglioma, metastatic disease), the choline to creatine ratio ranged from 0.36 to 4.38 (mean $\pm\, \sigma = 2.0 \pm 0.2$). Thus, there was substantial overlap in choline to creatine ratios among normal tissue, non-neoplastic lesions and malignant tumors. With regard to similar problems of relying upon values of choline to creatine and choline to NAA ratios, Howe and Opstad [35] conclude that although elevated ratios of choline to creatine and to NAA are typically found in tumors, these characteristics must be used cautiously, since other lesions may exhibit similar features.

Although much of MRS-based brain tumor diagnostics has relied upon metabolite ratios, these ratios are affected by a number of confounding factors [4–6]. For example, since different metabolites have different relaxation times, metabolite ratios are dependent upon TE. Changes in TE greatly impact upon the usefulness of metabolite ratios for distinguishing various grades of brain tumors [27].

Moreover, the use of metabolite concentration ratios [A]/[B] is also problematic for accurate assignment of spectral changes to specific disease processes [36], since the denominator [B] often varies for reasons unrelated to the oncologic process of interest. For example, the ratio of choline to NAA, upon which detection of brain tumor is heavily based in proton MRS, may also be due to loss of NAA, which is seen in a fairly wide variety of neurological disorders including epilepsy, multiple sclerosis, as well as in cerebrovascular accidents [22]. Moreover, high NAA can occur with contamination from non-malignant tissues in the vicinity of brain tumors [37]. Alteration in the ratios of choline to NAA and to creatine may also occur as a result of sub-clinical neurotoxicity related to chemotherapy, possibly due to neuronal loss and/or inhibition of cell metabolism, as well as to radiation effects [12,38]. There is also a wide variation in metabolic ratios in normal brain, especially comparing white and gray matter [22,26]. Thus, exclusive reliance on a ratio, where a change in the denominator could be due to a non-malignant process, especially one directly related to the therapy, could severely hamper the ability to use MRS and MRSI to reliably monitor response of tumor to therapy.

4.2 Reasons for the lack of reliability of metabolite concentration ratios obtained by conventional signal processors

The use of metabolite ratios in MRS and MRSI for neuroradiology has been extensive mainly due to difficulties in quantifying the actual metabolites of interest. These

difficulties can be traced back to the dominant use of the fast Fourier transform (FFT) for signal processing. The FFT, as a non-parametric, linear processor, can only generate the total shape or envelope of spectral structures, but cannot provide quantification. This processor necessitates long acquisition times T of encoded exponentially damped complex-valued harmonics as free induction decay (FID) curves, in attempts to improve resolution, which is proportional to $1/T$. This is problematic, since measuring longer FIDs invariably corrupts the time data with more noise, which, in turn, worsens resolution, which one seeks to amend. This conundrum or "vicious circle", thereby brings insurmountable difficulties to the FFT, which, as a linear processor, exports the entire unsuppressed noise from the encoded (time) to the mathematically analyzed (frequency) domain.

The intrinsic lack of quantification capabilities of the FFT (i.e. the impossibility of directly providing the spectral parameters for each resonance, such as the peak position, height, width and phase) is usually handled in the MRS literature by post-processing the pre-computed Fourier envelopes using various fitting algorithms.[7] Any such fitting is inevitably biased and equivocal, since the unknown number of physical metabolites is pre-assigned by the user, rather than being dictated by the encoded FIDs in the process of quantifying reconstructions. By guessing the number of metabolites, fittings end up either over-modeling ("predicting" non-existent metabolites) or under-modeling (failing to identify metabolites that are actually present in the scanned tissue). Either case is diagnostically unacceptable because over-fitting (or under-fitting) would force any of the applied least-square minimizations to under-estimate (or over-estimate) all the peak areas that are otherwise proportional to the metabolite concentrations, in order to partially compensate for the errors due to extra (or missing) resonances, respectively. Having under-estimated or over-estimated the concentrations of all the individual metabolites entails errors in the corresponding concentration ratios.

Moreover, it is virtually impossible to have some sort of "lucky" compensation through cancellations of the opposite errors so that, in the end, fitting would produce the correct values of the sought ratios for concentrations of the diagnostically most relevant metabolites. At best, and the much more likely outcome of quantifications by fitting Fourier envelopes is to have unpredictable, i.e. random fluctuations possibly around the correct metabolite concentrations even when different users employ the same fitting algorithm for the same data. This is the case because subjective pre-selections of e.g. basis sets for the sought metabolites and their number in the LCModel inevitably vary from user to user. Consequently, the metabolite concentration ratios from fittings would be incoherently distributed (as reminiscent of random noise which, by definition, lacks any of the correlation features) around the associated proper values. This is the main reason for which the available data base from the MRS literature used in the present study for the metabolite concentration ratios and cutpoints (all based on quantification for the FFT spectra by fitting) has been found to lack sufficient diagnostic accuracy.

[7] Some of the algorithms using in MRS are: AMARES = Advanced Method for Accurate Robust and Efficient Spectral fitting, LCModel = Linear Combination of Model in vitro Spectra and VARPRO = variable projection method.

4.3 Rescue via more advanced, mathematically-optimized quantification of MRS/MRSI data

In our previous studies [6,39–43], we thoroughly and systematically dealt with the general problem of a mathematical optimization as it applies to medical diagnostics by means of MRS. Magnetic resonance spectroscopy is one of the key modalities particularly in cancer diagnostics, due to its non-invasiveness and lack of ionizing radiation. For this reason, MRS can be repeatedly used not only in diagnostics, but also for screening. The literature of MRS has already made important strides especially for brain, breast, ovarian and prostate cancer, malignancies that are of major public health concern. This noteworthy initial success has been achieved on the basis of only a handful of clinically relevant metabolites, the concentrations of which can be extracted from time signals encoded from patients. Despite these encouraging developments, MRS has not yet reached the stage of being a routine modality in widespread clinical use in cancer diagnostics. The principal reasons for this are:

(i) lack of uniform mathematical optimization, and
(ii) difficulties in separating noise from the physical content of the measured time signals.

Both these obstacles have successfully been bridged in Refs. [6,40–43] by applying the fast Padé transform, the FPT.

The importance of this line of research has been highlighted at e.g. the expert meeting on MRS for oncology, held by the U.S. National Cancer Institute [44], as well as at a special conference on Data Processing in MRS and MRI by the International Society for Magnetic Resonance in Medicine [45]. These developments within the arena of clinical oncology undoubtedly reflect an appreciation of the limitations of the customary "Fourier plus fitting" approaches within MRS.

As emphasized, the fast Fourier transform can provide only an overall total shape spectrum in the frequency domain, which represents an envelope of all the existing metabolite concentrations. The goal, however, is to precisely extract the information which is underneath this envelope, namely the component spectrum for each metabolite. Since this is impossible within the FFT itself, the customary procedure has been to resort to fitting the total shape spectrum from the FFT by adjusting the entire envelope to a pre-selected number of components. In so doing, the number of metabolites is fixed prior to the analysis. Subsequently, the concentrations of metabolites are estimated by various least square fitting techniques.

The major drawback of this usual procedure in MRS is the lack of uniqueness, since any number of pre-assigned peaks can be fitted to a given envelope within a prescribed accuracy. This procedure has not met with sufficient success in clinical applications because, as stated, physical metabolites are missed and unphysical ones are spuriously detected by fitting. With regard to point (ii) above, besides imparting noise unaltered from the time domain to the frequency domain due to its linearity, the FFT has no possibility of separating noise from the true signal. Each metabolite has one or more resonant frequencies. A task is to reconstruct these frequencies, known as chemical shifts. The FFT cannot retrieve them, since this method deals with the pre-fixed Fourier grid frequencies as a function of the total acquisition time T. Overall, the FFT by

itself cannot reconstruct chemical shifts of metabolites or metabolite concentrations, since it only provides the total shape spectra. This is why, in practice, such spectra are typically post-processed via the above-mentioned fitting procedures, with all the outlined drawbacks.

4.3.1 The way in which the FPT provides quantification through the unique solution to the inverse harmonic problem

The fast Padé transform simultaneously circumvents all the listed drawbacks of the fast Fourier transform, and the associated fittings. As a non-linear transform, the FPT suppresses noise from the analyzed time signals. Most importantly, the FPT avoids post-processing altogether whether by fitting or by any other subjective adjustments. This is accomplished by direct quantification of the given time signal through exact spectral quantum-mechanical analysis, which provides the unique solution for the inverse harmonic problem. This solution contains four real-valued spectral parameters (two for the complex frequency ω_k and two for the associated complex amplitude d_k) for each resonance or peak in the corresponding frequency spectrum. Such an outcome of the Padé-based spectral analysis (quantification) represents the complete parametrization of the encoded FID, $\{c_n\}$, by means of the sum of K physical resonances:

$$c_n = \sum_{k=1}^{K} d_k \mathrm{e}^{i\omega_k \tau n}, \quad \mathrm{Im}(\omega_k) > 0 \quad (0 \le n \le N-1), \tag{5}$$

where τ is the sampling time and N is the total signal length ($\tau = T/N$). At any real frequency ω (chemical shift) the ensuing Padé spectrum $R(\omega)$ is fully determined by the rational function as a quotient of two polynomials P_K and Q_K of degree K:

$$R(z) = \frac{P_K(z)}{Q_K(z)}, \quad z = \mathrm{e}^{i\omega\tau}. \tag{6}$$

For the encoded time signal $\{c_n\}$, both polynomials P_K and Q_K are obtained by the exact convolution through solving one system of linear equations that emerges from the matching condition:

$$\sum_{n=0}^{N-1} c_n z^{-n} = \frac{P_K(z)}{Q_K(z)}. \tag{7}$$

The fundamental or nodal frequencies $\{\omega_k\}(0 \le k \le K-1)$ are obtained by rooting the denominator polynomial:

$$Q_K = 0 \Rightarrow \text{Spectral poles}. \tag{8}$$

The corresponding amplitudes $\{d_k\}(0 \le k \le K-1)$ are deduced from the Cauchy analytical formula for the residues of P_K/Q_K taken at $\omega = \omega_k$. The solutions of the

denominator characteristic equation (8) are the poles in the spectrum (6). The zeros in the spectrum (6) are the solutions of the numerator characteristic polynomial equation:

$$P_K = 0 \Rightarrow \text{Spectral zeros.} \tag{9}$$

Spectral zeros and poles suffice for the complete parametrization and quantification of MRS data in both time and frequency domains. The physical meaning of the rational polynomial P_K/Q_K is in representing the frequency-dependent response function of the scanned tissue which was externally perturbed by the radiofrequency excitation pulses in the presence of the static magnetic field of strength B_0. It is through this response function that we can peer into the physico-biochemical content of the examined tissue to gain information for medical diagnostics. As stated, among the most diagnostically informative data are the molar concentrations of key metabolites that are present in the tissue. These concentrations can be unambiguously deduced from the Padé-reconstructed fundamental frequencies and amplitudes $\{\omega_k, d_k\}(0 \leq k \leq K-1)$ [6,39–43].

The true number of physical resonances is also in the linelist of the exact reconstructions by the FPT. As opposed to conventional signal processing (FFT plus fitting), K is not guessed in the FPT. Rather, the FPT determines the exact number K of metabolites in the course of quantifying the FID. This is done by initializing the spectral analysis from (7) by a number K_j to solve the system of linear equations for the expansion coefficients of polynomial P_{K_j} and Q_{K_j}. This gives a rough estimate of the K_j spectral parameters $\{\omega_k, d_k\}(0 \leq k \leq K_j)$. Subsequently, a sequence of quantifications is performed with the same FID by systematically enlarging K_j via K_{j+m} where m is a set of positive integers. For each increment m added to K_j, the reconstructed spectral parameters $\{\omega_k, d_k\}$ are monitored to evaluate their stability. Computation is stopped at $m = M$ at which all the retrieved parameters $\{\omega_k, d_k\}$ $(0 \leq k \leq K_{j+M})$ are found to be stable. This also implies stability of the spectral shape in the FPT:

$$\frac{P_{(K_j+M)+M'}}{Q_{(K_j+M)+M'}} = \frac{P_{K_j+M}}{Q_{K_j+M}} \quad (M' = 1, 2, \ldots). \tag{10}$$

In other words, identical component spectra for each stable resonance as well as for the total shape spectrum are obtained for any M' above the total number K_T of all the retrieved resonances:

$$K_T = K_j + M. \tag{11}$$

Nevertheless, this does not mean that K_T is equal to the exact number K_G of genuine fundamental harmonics for K physical resonances $(K = K_G)$. Quite the contrary happens, since practice shows that the total number of found resonances in any signal processor is much larger than the true number K_G of genuine resonances:

$$K_T >> K_G. \tag{12}$$

4.3.2 Distinguishing physical from unphysical resonances by means of the FPT

If the sought exact Padé spectrum, built exclusively from genuine resonances $\{\omega_k, d_k\}(0 \leq k \leq K_G)$, is given by P_{K_G}/Q_{K_G}, in the face of inequality (12), or merely $K_T > K_G$, a key question is raised as to precisely how the stability condition (10) could be fulfilled:

$$\frac{P_{K_T}}{Q_{K_T}} = \frac{P_{K_G}}{Q_{K_G}} \quad (K_T > K_G). \tag{13}$$

If the excess $K_T - K_G$ is denoted by K_F, we can rewrite Eq. (13) as follows:

$$\frac{P_{K_G+K_F}}{Q_{K_G+K_F}} = \frac{P_{K_G}}{Q_{K_G}} \quad (K_T = K_G + K_F). \tag{14}$$

This gives a clear interpretation of the stability criterion: the excess of K_F resonances among the total number K_T of extracted resonances must necessarily be physically irrelevant, if (14) is to hold. Inspection of all the found parameters $\{\omega_k,\ d_k\}(0 \leq k \leq K_T)$ reveals that only a small portion of them are indeed stable, whereas the majority fluctuate with even the slightest change in e.g. the degree of the Padé polynomials. At this point in the analysis, we bin the reconstructed data into two distinct categories: stable and unstable. Stable resonances are classified as physical (genuine) and their number is given by K_G. The remaining $(K_T - K_G)$ unstable resonances are unphysical (spurious) and their number is K_F:

$$K_F = K_T - K_G. \tag{15}$$

Discarding the irrelevant K_F resonances from the full output list, we retain only the truly physical content of the Padé-reconstructed spectral parameters:

$$\{\omega_k, d_k\} \qquad (0 \leq k \leq K_G). \tag{16}$$

Nevertheless, the analysis is not yet completed, until the explanation is given as to precisely how these K_F unstable resonances are annihilated in such a thorough manner that no trace whatsoever of their presence is left on either the individual component spectra or on the total envelope, as per 14). Some sort of opposite or counteracting effects that cancel out the contribution of the K_F spectral structures to the component and total shape spectra must have eliminated these spurious resonances.

Indeed, this is what actually happens in $P_{K_G+K_F}/Q_{K_G+K_F}$ from (14), where the spurious contents in the numerator $P_{K_G+K_F}$ and denominator $Q_{K_G+K_F}$ coincide, and, therefore, cancel each other. This leaves only the physical resonances P_{K_G}/Q_{K_G} as the stabilized spectrum on the rhs of Eq. (14). The identical level of spuriousness in both $P_{K_G+K_F}$ and $Q_{K_G+K_F}$ is due to the exact confluence of the K_F subset of the total $K_G + K_F$ solutions of characteristic (or secular) polynomial equations:

$$P_{K_G+K_F} = 0 \Rightarrow z_{k,P} = \mathrm{e}^{i\tau\omega_{k,P}}, \tag{17}$$

$$Q_{K_G+K_F} = 0 \Rightarrow z_{k,Q} = \mathrm{e}^{i\tau\omega_{k,Q}}. \tag{18}$$

Here, the subscripts P and Q in the harmonic variable z_k and frequency ω_k refer to the numerator and denominator polynomial, respectively. In other words, mechanism (14) of the mentioned compensating effects that eliminate the K_F spurious resonances from the spectrum $P_{K_G+K_F}/Q_{K_G+K_F}$ consists of the emergence of harmonic pairs (or Froissart doublets) $z^F_{k,P}$ and $z^F_{k,Q}$ that have the same values:

$$z^F_{k,P} = z^F_{k,Q} \,(\text{maximal}\, k = K_F)\,. \tag{19}$$

Superscript F refers to Froissart, to honor the originator who discovered pole-zero coincidences for spurious structures in simple numerical experiments within the Padé approximant [6,39–41].

Likewise, we can denote the genuine harmonic variables and frequencies by $z^G_{k,P}$ and $z^G_{k,Q}$ as well as $\omega^G_{k,P}$ and $\omega^G_{k,Q}$, respectively, that are from the complementary subset of K_G stable resonances. These harmonics $z^G_{k,P}$ and $z^G_{k,Q}$ are the K_G roots of Eqs. (17) and (18), respectively. The union of the subsets of the binned spectral zeros and poles represents the collections of all the $K_G + K_F$ found zeros and poles:

$$\left\{z_{k,P}\right\} = \left\{z^G_{k,P}\right\} + \left\{z^F_{k,P}\right\}, \tag{20}$$

$$\left\{z_{k,Q}\right\} = \left\{z^G_{k,Q}\right\} + \left\{z^F_{k,Q}\right\}. \tag{21}$$

Once all the roots of the characteristic polynomials (17) and (18) become available, both $P_{K_G+K_F}$ and $Q_{K_G+K_F}$ can be written in their canonical forms:

$$\frac{P_{K_G+K_F}}{Q_{K_G+K_F}} \propto \prod_{k=1}^{K_G+K_F} \frac{(z - z_{k,P})}{(z - z_{k,Q})}. \tag{22}$$

The constant pre-multiplying factor which is the ratio of the expansion coefficients of the highest power $z^{K_G+K_F}$ in the numerator and denominator polynomial is left out, as inessential for this discussion. Regrouping the genuine and spurious harmonics in (22) according to the binning (20) and (21) yields:

$$\frac{P_{K_G+K_F}}{Q_{K_G+K_F}} \propto \left\{\prod_{k=1}^{K_G} \frac{(z - z^G_{k,P})}{(z - z^G_{k,Q})}\right\} \left\{\prod_{k'=1}^{K_F} \frac{(z - z^F_{k',P})}{(z - z^F_{k',Q})}\right\}. \tag{23}$$

By reference to (19), the second product on the rhs of Eq. (23) is equal to unity and this is called pole-zero cancellation, which removes all the spurious resonances from the total spectrum, leading to:

$$\frac{P_{K_G+K_F}}{Q_{K_G+K_F}} \propto \prod_{k=1}^{K_G} \frac{(z - z_{k,P}^G)}{(z - z_{k,Q}^G)} = \frac{P_{K_G}}{Q_{K_G}}, \tag{24}$$

in agreement with (14), which was set to prove (QED).

The canonical representation (24) of the Padé rational polynomial is not the only demonstration that spurious resonances make no contribution to the spectrum. The canonical form relies only on frequencies. An alternative demonstration can also be used in terms of both frequencies and amplitudes $\{\omega_k, d_k\}$ in the Heaviside partial fraction decomposition of $P_{K_G+K_F}/Q_{K_G+K_F}$. This time, the part of the partial fractions containing spurious resonances will disappear altogether due to their zero-valued amplitudes:

$$d_k^F = 0 \quad \text{(Amplitudes of spurious resonances)}\,. \tag{25}$$

This is a direct consequence of the definition and meaning of spectral amplitude which, as a metric, is related to the distance between a pole and a zero:

$$d_k \propto z_{k,Q} - z_{k,P}. \tag{26}$$

For Froissart doublets, poles and zeros coincide, as per (19), so that:

$$d_k^F \propto z_{k,Q}^F - z_{k,P}^F = 0 \quad (z_{k,Q}^F = z_{k,P}^F). \tag{27}$$

As such, the FPT possesses a twofold signature identifying spurious resonances: pole-zero coincidences (19) and zero-valued amplitudes (27). In practice, the easiest way to first spot spurious resonances in a long list of Padé-reconstructed spectral parameters is to look for amplitudes that are nearly zero-valued. Subsequent cross checking to detect the corresponding pole-zero confluences ($\omega_{k,P} \approx \omega_{k,Q}$) is the second verification for identifying Froissart doublets. It is in this robust and comprehensive way that the fast Padé transform first performs quantification and then separates the genuine from noise and noise-like information.

4.4 Potential clinical implications of Padé-optimized quantification of MRS/MRSI data in radiation neuro-oncology

In summary, the clinically most important information, the metabolite concentrations are unequivocally extracted from these spectral parameters, thus bypassing the ambiguities from fittings (under-fitting associated with missing genuine metabolites and over-fitting corresponding to the production of unphysical resonances). Furthermore, the FPT succeeds in solving the most difficult problem in spectral analysis of time signals corrupted with noise by providing exact separation of signal from noise. Identification of noise and noise-like information is achieved in the FPT through the appearance of Froissart doublets where poles and zeros coincide in the processed spectrum. As a double signature for signal-noise separation, the FPT detects zero-valued amplitudes

for Froissart doublets. In this way, genuine and spurious resonances are unmistakably disentangled within the FPT.

The enumerated major features of the FPT have been systematically tested using both theoretically generated and experimentally measured time signals. The FPT was found to work with remarkable success for synthesized time signals through machine accurate reconstructions of all the input spectral parameters as well as the number of resonances [6,39–41].

For experimentally measured time signals, the FPT is also highly successful as evidenced most recently e.g. for the encoded FIDs from the human brain [46]. Our other reported results [47–50] confirm the overall reliable performance of the FPT for time signals typical of data encoded from ovary, prostate and breast, both benign and malignant. Such findings were previously lacking in the MRS literature for these specific problem areas. Moreover, Refs. [6,42,46] on the fast Padé transform demonstrate that more advanced mathematical methods are vital to such applications that are relevant to major human health concerns.

The fast Padé transform has been shown to be particularly appropriate for in vivo MRS and MRSI, as applied to neuroradiology [5,6,46]. Compared to the conventional Fourier-based methods, the fast Padé transform has also been demonstrated to provide more reliable values of metabolite ratios that could potentially be used for improved target definition in radiation neuro-oncology [46,51].

It was noted that all the MRS data concerning lactate were obtained using very long echo times ($\geq$270 ms). At short TE, there may be overlap with lipids, that like lactate, also resonate at $\sim$1.3 ppm. Several other clinically important metabolites in brain tumor diagnostics are known to decay rapidly and can, therefore, only be seen at short TE [22]. The capability of the fast Padé transform to delineate and precisely quantify closely overlapping resonances could be particularly useful herein. Namely, MRS with short echo time could be used to reveal a more extensive panoply of metabolites that best distinguish recurrent brain tumors from radiation necrosis.

By analyzing a substantial number of MR time signals via the fast Padé transform, databases could be developed to provide standards of metabolite concentrations and also their ratios, so that recurrent brain tumors post-RT could be most reliably distinguished from radiation necrosis. Generating these accurate standards would be the indispensable next step aimed at solving this urgent problem in radiation neuro-oncology. Via Padé-based optimization, the power of in-depth multivariate assessment could then be fully exploited to explore the rich metabolic information provided by the entire MR spectrum.

5 Conclusions

Each of the metabolite ratios significantly distinguished recurrent tumor from radiation necrosis after radiation therapy. Nevertheless, the presented meta-analysis did not identify any metabolite ratios that unequivocally differentiate these two entities, nor were any optimal metabolite ratio cutpoints identified, even with adjustment for echo time, magnetic field strength and grade of the primary tumor. Much of MRS-based brain tumor diagnostics has relied upon metabolite ratios, although these ratios are influenced by many confounding factors. Most fundamentally, reliable quantification

of MRS data is the precondition for computed metabolite ratios to consistently yield the best possible diagnostic accuracy. The main reason for the lack of the sought diagnostic accuracy is due to the exclusive use of equivocal fitting in order to post-process the Fourier envelope spectra. All the fitting techniques in the MRS/MRSI literature begin by simply surmising the number of reconstructed physical metabolites leading to over-or under-estimated concentrations of the remaining retrieved metabolites. Invariably, this introduces bias and random errors into the sought ratios of such metabolite concentrations. The key to overcoming this problem is to identify the true metabolites and compute their correct concentrations, while simultaneously detecting and discarding all unphysical information arising from either noise or signal processing artefacts. This more advanced mathematical approach via the fast Padé transform is known to yield the correct metabolite concentrations from which the actual ratios are systematically generated. It is this kind of strategy which could ascertain the degree to which metabolite ratios might be diagnostically useful. Thus far, with Fourier-based signal processing, barely 2–4 concentration ratios of metabolites have been considered as diagnostically informative. This is clearly an over-simplification of the overall potential of MRS/MRSI. Much richer information for each encoded time signal is routinely provided by the fast Padé transform, without any fitting, through the output linelist of accurately retrieved spectral parameters (peak positions, heights, widths and phases) of every resonance for more than 20 genuine metabolites. We anticipate that using such a comprehensive database of mathematically optimized Padé-based reconstructions will substantially improve the identification of recurrent brain tumor post-RT as opposed to radiation-induced changes such as necrosis and the like.

Acknowledgments This work was supported by Cancerfonden, the King Gustav the 5th Jubilee Fund and the Karolinska Institute Fund, to which the authors are grateful and to the COST action MP 1002 "Nanoscale insight in ion-beam cancer therapy".

References

1. B. Palumbo, Brain tumour recurrence: brain single-photon emission computerized tomography, PET and proton magnetic resonance spectroscopy. Nucl. Med. Commun. **29**, 730–735 (2008)
2. M. Chorvath, E. Boljesikova, L. Pruzincova, V. Procka, B. Rychly, M. Novotny, P. Kalina, V. Belan, I. Makaiova, J. Steno, Post-therapeutical changes in the brain: novel trends in imaging and their influence on external beam radiotherapy. Neoplasma **56**, 156–162 (2009)
3. C.R. Kelsey, S. Mukundan, Z. Wang, C.A. Hahn, B.J. Soher, J.P. Kirkpatrick, Assessing neurotoxicity from the low-dose radiation component of radiosurgery using magnetic resonance spectroscopy. Neuro-Oncology **12**, 145–152 (2010)
4. K. Belkić, *Molecular Imaging through Magnetic Resonance for Clinical Oncology* (Cambridge International Science Publishing, Cambridge, 2004)
5. K. Belkić, Dž. Belkić, Spectroscopic imaging through magnetic resonance for brain tumour diagnostics: recent achievements, dilemmas and potential solutions via advances in signal processing. J. Comput. Methods Sci. Eng. **4**, 157–207 (2004)
6. Dž. Belkić, K. Belkić, *Signal Processing in Magnetic Resonance Spectroscopy with Biomedical Applications* (Taylor & Francis Group, London, 2010)
7. K. Kamada, K. Houkin, H. Abe, Y. Sawamura, T. Kashiwaba, Differentiation of cerebral radiation necrosis from tumor recurrence by proton magnetic resonance spectroscopy. Neurol. Med. Chir. (Tokyo) **37**, 250–256 (1997)
8. E. Matsusue, J.R. Fink, J.K. Rockhill, T. Ogawa, K.R. Maravilla, Distinction between glioma progression and post-radiation change by combined physiologic MR imaging. Neuroradiology **52**, 297–306 (2010)

9. T. Nakajima, T. Kumabe, M. Kanamori, R. Saito, M. Tashiro, M. Watanabe, T. Tominaga, Differential diagnosis between radiation necrosis and glioma progression using sequential proton magnetic resonance spectroscopy and methionine positron emission tomography. Neurol. Med. Chir. (Tokyo) **49**, 394–401 (2009)
10. C. Peca, R. Pacelli, A. Elefante, M.L. DelBassoDe Caro, P. Vergara, G. Mariniello, A. Giamundo, F. Maiuri, Early clinical and neuroradiological worsening after radiotherapy and concomitant temozolomide in patients with glioblastoma: Tumour progression or radionecrosis? Clin. Neurol. Neurosurg. **111**, 331–334 (2009)
11. R. Prat, I. Galeano, A. Lucas, J.C. Martínez, M. Martín, R. Amador, G. Reynés, Relative value of magnetic resonance spectroscopy, magnetic resonance perfusion, and 2-(18F) fluoro-2-deoxy-D-glucose positron emission tomography for detection of recurrence or grade increase in gliomas. J. Clin. Neurosci. **17**, 50–53 (2010)
12. J.D. Rabinov, P. Lani Lee, F.G. Barker, D.N. Louis, G.R. Harsh, G.R. Cosgrove, E.A. Chiocca, A.F. Thornton, J.S. Loeffler, J.W. Henson, R.G. Gonzalez, In vivo 3-T MR spectroscopy in the distinction of recurrent glioma versus radiation effects: initial experience. Radiology **225**, 871–879 (2002)
13. J.P. Rock, D. Hearshen, L. Scarpace, D. Croteau, J. Gutierrez, J.L. Fisher, M.L. Rosenblum, T. Mikkelsen, Correlations between magnetic resonance spectroscopy and image-guided histopathology, with special attention to radiation necrosis. Neurosurgery **51**, 912–920 (2002)
14. L.L. Wald, S.J. Nelson, M.R. Day, S.E. Noworolski, R.G. Henry, S.L. Huhn, S. Chang, M.D. Prados, P.K. Sneed, D.A. Larson, W.M. Wara, M. McDermott, W.P. Dillon, P.H. Gutin, D.B. Vigneron, Serial proton magnetic resonance spectroscopy imaging of glioblastoma multiforme after brachytherapy. J. Neurosurg. **87**, 525–534 (1997)
15. P. Weybright, P. Maly, D. Gomez-Hassan, C. Blaesing, P.C. Sundgren, MR spectroscopy in the evaluation of recurrent contrast-enhancing lesions in the posterior fossa after tumor treatment. Neuroradiology **46**, 541–549 (2004)
16. P. Weybright, P. Sundgren, P. Maly, D. Gomez-Hassan, B. Nan, S. Rohrer, L. Junck, Differentiation between brain tumor recurrence and radiation injury using MR spectroscopy. Am. J. Radiol. **185**, 1471–1476 (2005)
17. J. Walecki, E. Tarasów, B. Kubas, Z. Czernicki, J. Lewko, J. Podgórski, M. Sokól, P. Grieb, Hydrogen-1 MR spectroscopy of the peritumoral zone in patients with cerebral glioma: assessment of the value of the method. Acad. Radiol. **10**, 145–153 (2003)
18. Q.-S. Zeng, C.-F. Li, H. Liu, J.-H. Zhen, D.-C Feng, Distinction between recurrent glioma and radiation injury using magnetic resonance spectroscopy in combination with diffusion-weighted imaging. Int. J. Radiat. Oncol. Biol. Phys. **68**, 151–158 (2007)
19. Q.-S. Zeng, C.-F. Li, K. Zhang, H. Liu, X.-S. Kang, J.-H. Zhen, Multivoxel 3D proton MR spectroscopy in the distinction of recurrent glioma from radiation injury. J. Neurooncol. **84**, 63–69 (2007)
20. E.A. Smith, R.C. Carlos, L.R. Junck, C.I. Tsien, A. Elias, P.C. Sundgren, Developing a clinical decision model: MR spectroscopy to differentiate between recurrent tumor and radiation change in patients with new contrast-enhancing lesions. Am. J. Radiol. **192**, W45–W52 (2009)
21. P.E. Sijens, M. Oudkerk, ^{1}H chemical shift imaging characterization of human brain tumor and edema. Eur. Radiol. **12**, 2056–2061 (2002)
22. L.A. Brandão, R.C. Domingues, *MR Spectroscopy of the Brain* (Lippincott Williams & Wilkins, Philadelphia, 2004)
23. S. Siegel, *Non-parametric Statistical Analysis* (McGraw-Hill Kogahusha Ltd., Tokyo, 1956)
24. J.F. Hair, R.E. Anderson, R.L. Tatham, W.C. Black, *Multivariate Data Analysis*, 5th edn. (Prentice-Hall International, Inc, London, 1998)
25. D.W. Hosmer, S. Lemeshow, *Applied Logistic Regression*, 2nd edn. (Wiley, New York, 2000)
26. E.R. Danielsen, B. Ross, *Magnetic Resonance Spectroscopy Diagnosis of Neurological Diseases* (Marcel Dekker, Inc., New York, 1999)
27. M. Kaminogo, H. Ishimaru, M. Morikawa, M. Ochi, R. Ushijima, M. Tani, Y. Matsuo, J. Kawakubo, S. Shibata, Diagnostic potential of short echo time MR spectroscopy of gliomas with single-voxel and point-resolved spatially localized proton spectroscopy of brain. Neuroradiology **43**, 353–363 (2001)
28. C.K. Kim, B.K. Park, Update of prostate magnetic resonance imaging at 3T. J. Comput. Assist. Tomogr. **32**, 163–172 (2008)
29. R. Tarnawski, M. Sokol, P. Pieniazek, B. Maciejewski, J. Walecki, L. Miszczyk, T. Krupska, ^{1}H-MRS in vivo predicts the early treatment outcome of postoperative radiotherapy for malignant gliomas. Int. J. Radiat. Oncol. Biol. Phys. **52**, 1271–1276 (2002)

30. A.P. Lin, B.D. Ross, Short-echo time proton MR spectroscopy in the presence of gadolinium. J. Comput. Assist. Tomogr. **25**, 705–712 (2001)
31. T.R. McKnight, M.H. Bussche, D.B. Vigneron, Y. Lu, M.S. Berger, M.W. McDermott, W.P. Dillon, E.E. Graves, A. Pirzkall, S.J. Nelson, Histopathological validation of a three-dimensional magnetic resonance spectroscopy index as a predictor of tumor presence. J. Neurosurg. **97**, 794–802 (2002)
32. R. Hourani, L.J. Brant, T. Rizk, J.D. Weingart, P.B. Barker, A. Horska, Can proton MR spectroscopic and perfusion imaging differentiate between neoplastic and nonneoplastic brain lesions in adults? Am. J. Neuroradiol. **29**, 366–372 (2008)
33. C. Majós, C. Aguilera, J. Alonso, M. Julia-Sape, S. Castener, J.J. Sanchez, A. Samitier, A. Leon, A. Rovira, C. Arús, Proton MR spectroscopy improves discrimination between tumor and pseudo-tumoral lesions in solid brain masses. Am. J. Neuroradiol. **30**, 544–551 (2009)
34. J.K. Smith, A. Londono, M. Castillo, L. Kwock, Proton magnetic resonance spectroscopy of brain-stem lesions. Neuroradiology **44**, 825–829 (2002)
35. F.A. Howe, K.S. Opstad, ^{1}H spectroscopy of brain tumours and masses. NMR Biomed. **16**, 123–131 (2003)
36. P.A. Bottomley, The trouble with spectroscopy papers. J. Magn. Reson. Imaging **2**, 1–8 (2002)
37. D. Vigneron, A. Bollen, M. McDermott, L. Wald, M. Day, S. Moyher-Noworolski, R. Henry, S. Chang, M. Berger, W. Dillon, S. Nelson, Three-dimensional magnetic resonance spectroscopic imaging of histologically confirmed brain tumors. Magn. Reson. Imaging **19**, 89–101 (2002)
38. B. Ciskowska-Lyson, L. Krolicki, A. Teska, A. Janowicz-Zebrowska, K. Zajda, M. Krzakowski, E. Tacikowska, Proton magnetic resonance spectroscopy investigations in brain metabolic changes after first doses of chemotherapy. MAGMA **15**(Suppl.1), 149 (2002)
39. Dž. Belkić, *Quantum Mechanical Signal Processing and Spectral Analysis* (Institute of Physics Publishing, Bristol, 2005)
40. Dž. Belkić, Exact quantification of time signals in Padé-based magnetic resonance spectroscopy. Phys. Med. Biol. **51**, 2633–2670 (2006)
41. Dž. Belkić, Exponential convergence rate (the spectral convergence) of the fast Padé transform for exact quantification in magnetic resonance spectroscopy. Phys. Med. Biol. **51**, 6483–6512 (2006)
42. Dž. Belkić, K. Belkić, Decisive role of mathematical methods in early cancer diagnostics: Optimized Padé-based magnetic resonance spectroscopy. J. Math. Chem. **42**, 1–35 (2007)
43. Dž. Belkić, K. Belkić, Unequivocal disentangling genuine from spurious information in time signals: Clinical relevance in cancer diagnostics through magnetic resonance spectroscopy. J. Math. Chem. **44**, 887–912 (2008)
44. J. Evelhoch, M. Garwood, D. Vigneron, M. Knopp, D. Sullivan, A. Menkens, L. Clarke, G. Liu, Expanding the use of magnetic resonance in the assessment of tumor response to therapy. Cancer Res. **65**, 7041–7044 (2005)
45. Data processing in MRS and MRI. International Society for Magnetic Resonance in Medicine. www.ismrm.org.workshops/data06/indix.htm
46. Dž. Belkić, K. Belkić, Practical improvements in medical diagnostics by mathematically-optimized MRS. J. Math. Chem. **49**, 2408–2440 (2011)
47. Dž. Belkić, K. Belkić, Mathematical modeling of an NMR chemistry problem in ovarian cancer diagnostics. J. Math. Chem. **43**, 395–425 (2008)
48. Dž. Belkić, K. Belkić, Unequivocal resolution of multiplets in MR Spectra for prostate cancer diagnostics achieved by the fast Padé transform. J. Math. Chem. **45**, 819–858 (2009)
49. Dž. Belkić, K. Belkić, Exact quantification of time signals from magnetic resonance spectroscopy by the fast Padé transform with applications to breast cancer diagnostics. J. Math. Chem. **45**, 790–818 (2009)
50. K. Belkić, Dž. Belkić, Possibilities for improved early breast cancer detection by Padé-optimized magnetic resonance spectroscopy. Isr. Med. Assoc. J. **13**, 236–243 (2011)
51. Dž. Belkić, K. Belkić, in *Molecular imaging and magnetic resonance for improved target definition in radiation oncology*, ed. by G García Gómez-Tejedor, MC Fuss Radiation Damage to Biomolecular Systems (Springer, Heidelberg, 2012), pp. 411–430